Experiments in Fluids 33 (2002) 709–719
DOI 10.1007/s00348-002-0536-2

Turbulence time scales in mixing box experiments

K. Dohan, B.R. Sutherland

Abstract Laboratory experiments are performed to examine eddy time scales in turbulence generated by an oscillating grid in homogeneous fluid using tanks with varying depth and fixed high aspect ratio horizontal cross-section. For high ratios of depth to width, a mean circulation develops in the form of a pair of counter-rotating vortices. In a new technique, pearlescent dye is employed to measure eddy time scales and to determine their power law scaling dependence on the distance from the oscillating grid. Two scaling regimes are observed, one near the source of turbulence and one at intermediate depths. At intermediate depths, the scaling exponent is found to increase if the total fluid depth is larger. We discuss the significance of these results on the use of the law-of-the-wall scaling in the upper oceanic mixed layer.

1 Introduction

Though much has been learned about the dynamics of homogeneous, isotropic turbulence that is uniformly forced, in many physical systems turbulence is generated at a localized source and is affected by the presence of rigid boundaries. The decay with distance from a source is examined in wind tunnel ("grid generated" turbulence) experiments (Comte-Bellot and Corrsin 1971; Tennekes and Lumley 1972) and mixing box experiments ("oscillating grid" turbulence) (Turner 1973). In wind tunnel experiments, a uniform mean flow passing through a mesh creates local horizontally homogeneous turbulence. Averaged over planes, the turbulence parallel to the grid decays with distance and by the Taylor hypothesis with time as it is transported by the mean flow away from the source. Examination of the statistical properties of turbulence in these experiments is useful, for example, in examining turbulent wakes behind moving objects.

Mixing box experiments are useful in understanding the properties of turbulence in circumstances where there is no mean flow. The experiments are performed in an enclosed tank and fluid is supplied continuously with turbulent kinetic energy generated by rapid vertical oscillations of a horizontal grid of bars. As in wind tunnel experiments, the turbulence is shear-free and approximately horizontally isotropic and homogeneous. Unlike wind tunnel experiments, however, the supplied energy remains contained within the finite volume of the box. Steady state is achieved through a balance between the energy supplied and the energy lost internally and at the boundaries.

A large body of work has been devoted to investigating the spatial decay of turbulence in mixing box experiments including the works of Thompson and Turner (1975), and Hopfinger and Toly (1976). They found the following scaling dependence upon depth, z, measured from a virtual origin which lies close to the grid:

$$l\tilde{z}, \tag{1}$$

$$u\tilde{K}z^{-1}, \tag{2}$$

where l is the integral length scale of the turbulence, u is the rms horizontal velocity, and K, determined by Long (1978a), parameterizes the turbulent production by the grid. K depends on viscosity, ν, as well as on the stroke length, frequency, and mesh size of the oscillating grid (S, f, and M respectively). For an oscillating grid with square bars, $K \sim f S^{3/2} M^{1/2}$, whereas for cylindrical bars, $K \sim (SfM/\nu)^{1/3} f S^{3/2} M^{1/2}$.

Their experiments were performed in mixing boxes with a square horizontal cross-section and analyzed mostly with the use of single-point measurements, such as laser-Doppler anemometry or hot-wire probes.

In the experiments conducted for this article, a mixing box with a high aspect ratio (approximately 5:1) horizontal cross-section was used. As well as enabling a study of the effect of horizontal confinement upon the turbulence dynamics, the tank geometry allows us to employ a new technique to visualize and measure statistical properties of the entire turbulent flow field. This technique uses pearlescent dye and digital image processing to measure eddy time scales as a function of the distance from the oscillating grid throughout the flow field. The purpose of this paper is to use this technique to investigate the effects of the high aspect ratio geometry and the position of the bottom boundary upon the spatial dependence of turbulence time scales in a homogeneous fluid.

In Sect. 2, the experimental configuration and the analysis technique are described. Sections 2.1 and 2.2 detail the experimental set-up and the method by which the

Received: 6 July 2002 / Accepted: 8 August 2002
Published online: 26 September 2002

K. Dohan, B.R. Sutherland (✉)
Department of Mathematical and Statistical Sciences,
University of Alberta, Edmonton, AB, T6G 2G1, Canada
E-mail: bruce.sutherland@ualberta.ca

This work has been supported by the Natural Sciences and Engineering Research Council of Canada.

digital images are produced. Further processing of the images is described in Sects. 2.3 and 2.4 where the calculations of eddy time scales and velocities are described, respectively. Section 3 contains qualitative observations of the experiments. In Sect. 4, an alternate derivation to that given by Long (1978b) of the scaling theory for eddy time scales as a function of depth is presented. In Sect. 5, the eddy time-scale results and velocity measurements are provided along with the results to the theory of Sect. 4.

2 Experimental set-up and analysis

2.1 Apparatus

Experiments were performed in an acrylic tank of horizontal dimensions W=9.7 cm, L=47.6 cm, and of height H=49 cm as shown in Fig. 1a. The horizontal cross-section had a high aspect ratio compared with conventional experiments performed in tanks with square cross-sections. An acrylic "false bottom" was inserted horizontally at different levels so that the structure of turbulent eddies in fluid at differing depths could be examined. The tank was filled with water up to 2 cm from the top of the tank. A stainless steel mixer was inserted 7 cm from the top of the tank and 5 cm below the free surface of the water. The mixer was a ladder-shaped square grid of cylindrical bars of diameter 0.6 cm spaced 3.2 cm apart (solidity 27%) with "rungs" that extended beyond the struts of the ladder so that the ends of the bars extended to within 2 mm of the walls. The rungs extended 0.9 cm along the length and 2.6 cm along the width of the tank. When switched on, the mixer moved vertically up and down with a frequency of 7 Hz and with a peak-to-peak stroke length of 2.6 cm.

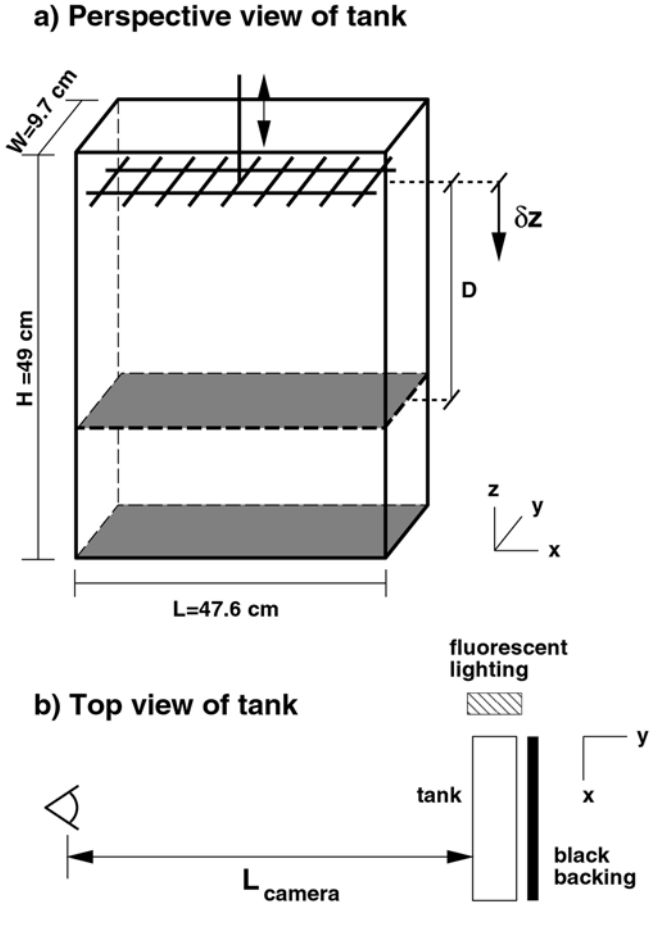

Fig. 1. The experimental set-up. The distance down from the midplane of the grid is denoted δz and the location of the replaceable bottom is at $\delta z=D$

A digital camera was positioned a distance $L_{\text{camera}} \approx 3$ m from the tank as shown in Fig. 1b. Black paper was fastened to the rear wall of the tank. A bank of fluorescent lights illuminated the interior of the tank through its left side from the point of view of the camera.

Figure 1a illustrates the coordinate system used in the discussion that follows: the downward distance from the grid is denoted by δz, which increases from zero at the mean vertical position of the mixer to the depth D ($\leq$ 42 cm) at the position of the false bottom; x is the distance from the left side; y is the distance from the front side of the tank, with respect to the camera's point of view.

The turbulent region was visualized using pearlescent dye (Mearlmaid Natural Pearl Essence AA, Thornley Co., Wilmington, Del.). Unlike typical dye-tracking techniques that identify motion by tracking the Lagrangian transport of the dye, pearlescence visualizes motion even when the dye is uniformly distributed throughout the fluid. The natural pearlescence used in this study is composed of microscopic (30×6 μm) reflective crystals obtained from fish scales. The crystals scatter light evenly throughout a stationary fluid but align with the eddy-induced shear once the fluid is in motion. This alignment with the shear visualizes the large turbulent eddy motions by reflecting the incident light in bright patches.

Although the specific gravity of the particles is 1.6, they are sufficiently small that their effect upon the flow is negligible. For example, the Stokes velocity of a falling sphere with the same density and with a diameter of 30 μm is 0.03 cm/s. This speed, which overestimates that of a falling plate, is a small fraction of the observed flow speeds. Likewise, the time over which co-aligned plates decorrelate owing to Brownian processes is negligibly small compared with the turbulence time scales.

Visualization of turbulence by reflective particles has been exploited, for example, by Voropayev and Fernando (1996) who used pearlescence, and by Dickinson and Long (1978) who observed turbulent fronts using suspended aluminum particles. An added advantage of our technique is that we not only visualize turbulent eddies, but we also compute eddy time and length scales from digitized images of the experiments.

The pearlescent dye was injected along the surface of the tank prior to the start of the experiment. After the mixer was turned on, the mixing region deepened and the dye was passively transported by the turbulent eddies. Thus, the dye simultaneously revealed the depth of the mixed region and the characteristics of the eddies themselves.

The images recorded by the digital camera are a weighted superposition of the turbulent motions across the width of the tank. Though the strongest signal came from eddies near the front of the tank, experiments

performed with a columnar beam illuminating a fraction of the width of the tank gave the same statistical results as those with the side wall fully illuminated. Thus, the camera predominantly recorded images of the interior eddy motions which were highlighted by the pearlescent dye, not the motions in the boundary layer of the front wall.

The recorded images in the x, z plane were analyzed using the image processing software package DigImage (Dalziel 1993). Snapshots of the experiment were digitized, enhanced, and analyzed using statistical methods. These methods are described in the following subsections.

2.2 Time series

A vertical time series is constructed by extracting a column of pixels at successive times from digitized images of the experiment as it evolves. The columns are positioned side by side to form a time series image. The time series can be constructed with a temporal resolution as small as 1/30 s (limited by the standard NTSC video frame rate). Up to 31 vertical time series (taken at 31 different horizontal positions) can be taken simultaneously. Likewise, one can construct horizontal time series.

Figure 2 shows a vertical time series for 1 min of an experiment with D=42 cm. The image is enhanced by representing intensities with a false color gray scale. The image shows the evolution of the mixing region along a vertical slice taken at a horizontal position x=16 cm from the left side of the tank and starting when the mixer is initially set in motion. The deepening of the mixed layer is marked by the vertical extent of the pearlescent dye which is initially at the level of the mixer and is transported downward as the turbulent region deepens. The figure shows that the mixed region deepens over the full depth of the tank after approximately 40 s. This time is consistent with that predicted by Dickinson and Long (1978; 1983).

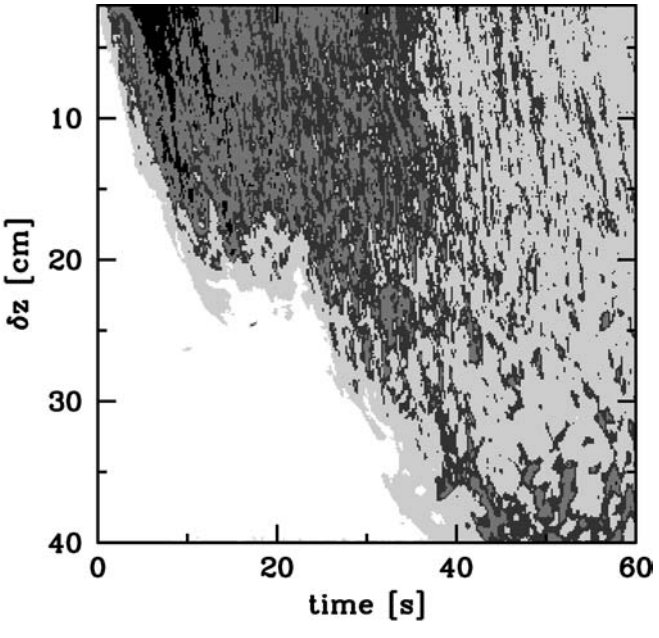

Fig. 2. Vertical time series showing the start of an experiment, taken 16 cm from left edge of tank. The field of view extends from just below the oscillating grid to the bottom boundary. A false colour scheme is used to display the image, with black representing the strongest intensities, grays representing weaker intensities, and white representing the weakest intensities

While deepening, the mean intensity of light incident upon the camera decreases as the pearlescent dye is diluted. The variations from the mean reveal eddy motions. A bright streak in the time series indicates the presence of an eddy in the field of view of the raw time series image. In particular, the dye shows an increase in turbulent eddy time scales from the top to the bottom of the mixed region where the streaks are broader at the bottom of the image. In this way, the width in time of any particular streak is a measure of the corresponding eddy turnover time and the slope of the streak measures the local vertical velocity in the turbulence. In a similar fashion, the horizontal velocities and time scales can be determined from horizontal time series.

Vertical time series are taken from the experimental images with a time step of 1/15 s and a duration of 30 s. This duration is chosen as a compromise between resolving the fast eddy motions and acquiring enough data for sufficient time averaging. In order to ensure that the time series included only the fully developed turbulence in statistically steady state, the time series are taken one minute into the experiment. The vertical extent of the time series is chosen to include the turbulent region of the time series while avoiding the mixer and the tank boundaries. Each time series is then passed through a high-pass Fourier filter in the horizontal direction to subtract the mean intensity from the digitized images. This removes the effects of light attenuation across the tank so that the resulting average intensity of each time series at each horizontal position is the same. Figure 3a shows a time series after these enhancements, displayed as a false color representation of the image.

2.3 Determination of time scales

We have used autocorrelations of intensity functions derived from (filtered) vertical time series to measure the eddy time scale as a function of the distance from grid.

We define a discrete function, $f_{\delta z}(t_n)$, as the variation in intensity over time at the vertical position, δz, from a vertical time series, where n is the (integer) time index. Explicitly, $t_n = n\Delta t$ for n=0, 1, ..., N, where Δt is the temporal resolution of the time series. Figure 3b and e shows typical profiles, $f_{\delta z}(t_n)$, for δz=10 and 35 cm, respectively. Both are taken from the time series in Fig. 3a along the cross-sections marked by the horizontal dotted lines. The location of strong eddies, marked as black in the time series image, show up as peaks in the intensity functions. The increase in eddy time scale with distance from the grid is evident because the peaks at δz=35 cm are much wider than those at δz=10 cm.

In general, for a discrete signal, $f(t_n)$, the autocorrelation is a discrete function of the (stepwise) temporal shift, $\tau_i \equiv i\Delta t$, defined by

$$A[f](\tau_i) = \sum_{n=i}^{N} f(t_n) f(t_n - \tau_i), \quad \tau : i = 0,\ 1,\ \ldots,\ N. \qquad (3)$$

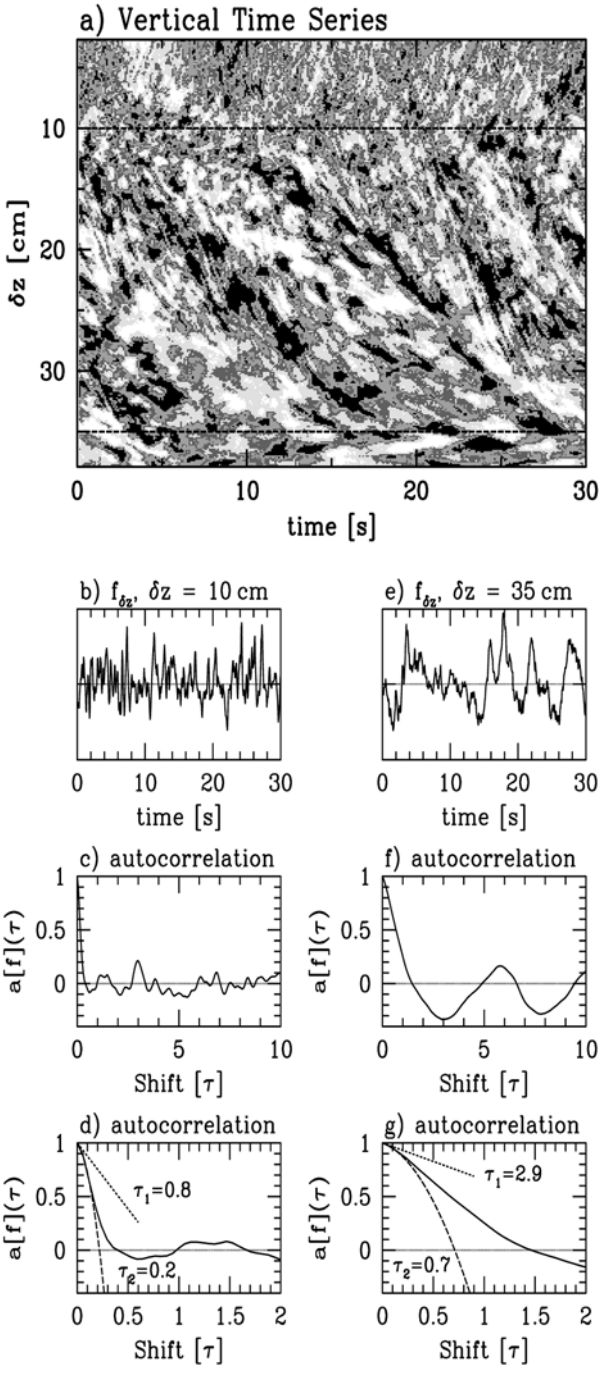

Fig. 3. **a** Vertical time series taken at x=16 cm in an experiment with D=42 cm. The same gray scale as in Fig. 2 is used. **b** Intensity plot in time at location 10 cm below grid. **c** Normalized autocorrelation of Fig. 3b. **d** Autocorrelation and tangent near shift τ=0. **e–g** Corresponding functions at location 35 cm below grid

The normalized autocorrelation is defined by $a[f](\tau)=A[f](\tau)/A[f](0)$. It is invariant to changes in scale of a function but is sensitive to a shift in the mean value. By setting the mean intensity to zero in each filtered time series, this sensitivity is removed.

Figure 3c and f shows the corresponding normalized autocorrelation functions of the signals in Fig. 3b and e, respectively. The narrow peaks in Fig. 3b result in a rapid decorrelation of the signal (the autocorrelation drops to zero within a small time shift). The wider peaks in Fig. 3e result in a slower decorrelation.

To characterize the eddy time scale we define two time scales based upon the behaviour of the autocorrelation function at τ=0.

We define the time scale based on the instantaneous change in the autocorrelation function about τ=0 to be

$$\mathscr{T}_1 = -\left(\frac{\mathrm{d}\, a[f](\tau)}{\mathrm{d}\tau}\bigg|_{\tau=0}\right)^{-1}. \tag{4}$$

Time scale $\mathscr{T}_1$ is an accurate measure of the widths of the peaks of an approximately piecewise constant function, but the time scale varies significantly as the discontinuities of the function become less pronounced and the changes from positive to negative values become more gradual. In fact, the tangent to the autocorrelation at τ=0 of a continuous function is horizontal, and $\mathscr{T}_1$ becomes infinite. For discrete signals, the derivative is calculated from the first three points of the autocorrelation and is zero only in the continuous limit.

The autocorrelation of a continuous time series has strictly negative curvature near τ=0. The first three terms in the Taylor series expansion of $a[f](\tau)$ about τ=0 are given by $1+a_1\tau+a_2\tau^2/2$, where $a_1=\mathrm{d}a[f](0)/\mathrm{d}\tau$ and $a_2=\mathrm{d}^2a[f](0)/\mathrm{d}\tau^2$. We can then define a second time scale as the τ intercept of this quadratic approximation to the value of $a[f](\tau)$. Explicitly,

$$\mathscr{T}_2 = \frac{-a_1 - \sqrt{a_1^2 2a_2}}{a_2}. \tag{5}$$

The time-scale definition of Eq. (5) is similar to the definition of the Taylor microscale for isotropic turbulence as described in Hinze (1959) although the functions that we are examining, rather than turbulence velocity components, are intensity functions which are related to the local shear in the flow.

If the signal is a piecewise linear function (as for a rapidly varying discretely sampled signal), $\mathscr{T}_1$ is the appropriate time scale. $\mathscr{T}_2$ is the appropriate time scale for a smoothly varying function and measures the characteristic width of the dominant peaks for a triangular wave. In particular, for a rectangular wave with period T, we find $\mathscr{T}_1 = T/4$. For a triangular wave with period T, we find $\mathscr{T}_2 = \sqrt{6}T/12$.

The autocorrelation functions in Fig. 3c and f are redrawn on a small τ scale in Fig. 3d and g, respectively. The tangents to $a[f](\tau)$ at τ=0 are superimposed as the dotted lines. The corresponding time scales $\mathscr{T}_1$ are the intercepts of these lines with the τ axis. The second order approximations to the curves are plotted as dashed lines. Note that $\mathscr{T}_1$ gives consistently higher values than $\mathscr{T}_2$ and that the intercepts of both time-scale curves with the τ axis are larger in the case δz=35 cm (Fig. 3g).

Using either method, a profile of time-scale value as it varies with distance from the midplane of the grid can be assembled for each time series by calculating the time scale associated with the intensity functions $f_{\delta z}(t_n)$ at increasing values of δz. A similar method could be used to determine the length scale in the turbulence at the time t_0 using

functions of position $f_{t0}(z_n)$, $z_n=\delta z_0+n\Delta z$, where Δz is the spatial resolution of the vertical time series.

The integral time scale (the integral of the normalized autocorrelation function) is the standard time-scale for turbulence measurements. This time-scale is inappropriate for our data since it assumes a negligible contribution to the integral by shifts far from the origin, whereas with our data non-negligible contributions to the integral will occur when two eddies overlap. This results in significant peaks in the autocorrelation function far from the origin, as seen in Fig. 3c and f. Similarly, the first zero crossing is not used as a time-scale since contributions from overlapping eddies may result in secondary peaks prior to the occurrence of the zero crossing.

Another standard technique in turbulence measurements is the Fourier transform. This method is also not applicable to our time series data. Results show that although there is a high-frequency cut-off at each vertical level, the edge of the cut-off is ambiguous and the power in the signal is spread throughout the lower frequencies without any clear peaks.

2.4
Velocity measurements

To measure velocity, consider two time-discretized signals $f_0(t_n)$ and $f_j(t_n)$, n=0, ±1, ±2... where, for notational convenience, $f_0 \equiv f_{\delta_{z_0}}$ and $f_j \equiv f_{\delta_{z_j}} = f_{\delta_{z_0+j\Delta z}}$. The cross-correlation is defined as a function of the temporal shift $\tau_i \equiv i\Delta t$ given by

$$C[f_0,\ f_j](\tau_i) = \sum_{n=\max(0,i)}^{\min(N,N+i)} f_0(t_n) f_j(t_n - \tau_i) \qquad (6)$$

where $|i| \le N$.

Eddies advected by a background flow appear as diagonal streaks in a vertical time series, the slopes of which provide the local background vertical velocities. Similarly, the slopes of streaks in a horizontal time series provide the local background horizontal velocities in the turbulence.

To extract the vertical velocity information from a vertical time series, a reference signal $f_0(t_n)$ is chosen as the intensity function at the position δz_0 in the time series taken along a vertical cross-section at $x=x_0$. Neighbouring signals $f_{-i}(t_n)$ and $f_i(t_n)$ are cross-correlated with $f_0(t_n)$ for a prescribed integer shift i. The smallest value τ at which $C[f_0,f_{-i}](\tau)$ is maximal is denoted by τ^-. Similarly τ^+ is the time shift for which $C[f_0,f_{+i}](\tau)$ is maximum. In practice, the critical points τ^+ and τ^- are each determined by quadratic interpolation of C from three points about τ=0. Finally, the average vertical velocity at δ_{z0} is estimated from the second order accurate derivative at τ=0 (hence where $\delta_z=\delta_{z0}$) for the function that passes through the three points (τ^-,δz_0–$i\Delta$z), (0,δz_0), (τ^+,δz_0+$i\Delta z$). Explicitly,

$$v(x_0, \delta z_0) = \frac{-i\Delta z}{(\tau^+ - \tau^-)}\left(\frac{\tau^+}{\tau^-} + \frac{\tau^-}{\tau^+}\right) \qquad (7)$$

This procedure is used to evaluate the vertical velocity at every vertical position, δz, along the time series. A Gaussian-weighted filter is used to determine the mean vertical velocity at a subset of vertical positions. Likewise, horizontal time series are used to determine horizontal velocities, and these are locally averaged to determine their values at the same spatial coordinates as the vertical velocities. Thus the velocity vector field is produced. In cases for which the mixing region exhibits a background circulation on a time scale longer than that of the turbulent eddies, the above method may be used to measure the velocity of the background flow. The technique effectively filters the fast time scale of the eddy motions and so provides an efficient method for determining the long time behaviour of the flow.

3
Observations

When the mixer was set in motion tiny jets and vortices were shed from the bars of the grid. Near the grid were small, fast eddies. Further below the grid the eddies persisted for longer times as they coalesced to form larger eddies and as viscosity damped the motion on small length and time scales. Depending upon the total depth of the tank, D, these eddies were further modified by a large-scale circulation that developed in the tank. If $D \gg W$, we observed that an overall circulation developed in the form of a pair of counter-rotating vortices oriented with vorticity vectors directed along the y axis (perpendicular to the long side of the tank). This circulation occurred in experiments with large values of D.

A sequence of horizontal time series for an experiment with D=42 cm is shown in Fig. 4. Figure 4a shows a horizontal time series taken at δz=6 cm, with each subsequent time series taken 4 cm further below the grid. The increase in horizontal eddy length scales is evident in the images. Near the bottom of the tank, the eddies are on the order of 2–3 cm. The overall circulation pattern can be detected from these images. A streak with a shallow slope corresponds to fast horizontal advection of an eddy, a negative slope corresponds to motion to the left and a positive slope corresponds to motion to the right of the tank. In all horizontal time series, except the two nearest the grid, there is a symmetric divergence of fluid from the centre of the tank toward the sides. As expected, at the edges there is almost no detectable horizontal motion. Near the grid (Fig. 4a) eddies exhibit less coherent fluctuations.

In experiments with $D \gg W$, the typical variations in vertical motions across the tank are illustrated in the nine vertical time series shown in Fig. 5 (from the same experiment as Fig. 4). The time series are taken starting 3.8 cm from the left side of the tank and are spaced 5 cm apart. As in Fig. 4, the increase in eddy time scales and length scales from the top to bottom of the tank is evident from the plots. The plots also show a change in vertical motions from large upward velocities at the sides (apparent by the positive slopes of the streaks), through a transition to downward velocities near the middle of the tank (apparent by the negative slopes). Although there are significant vertical motions throughout the tank, the fastest motions occur in the top half of the tank.

The two sets of time series illustrate the typical overall circulation which moved down the middle of the tank, left and right toward the sides, and rapidly upward along a

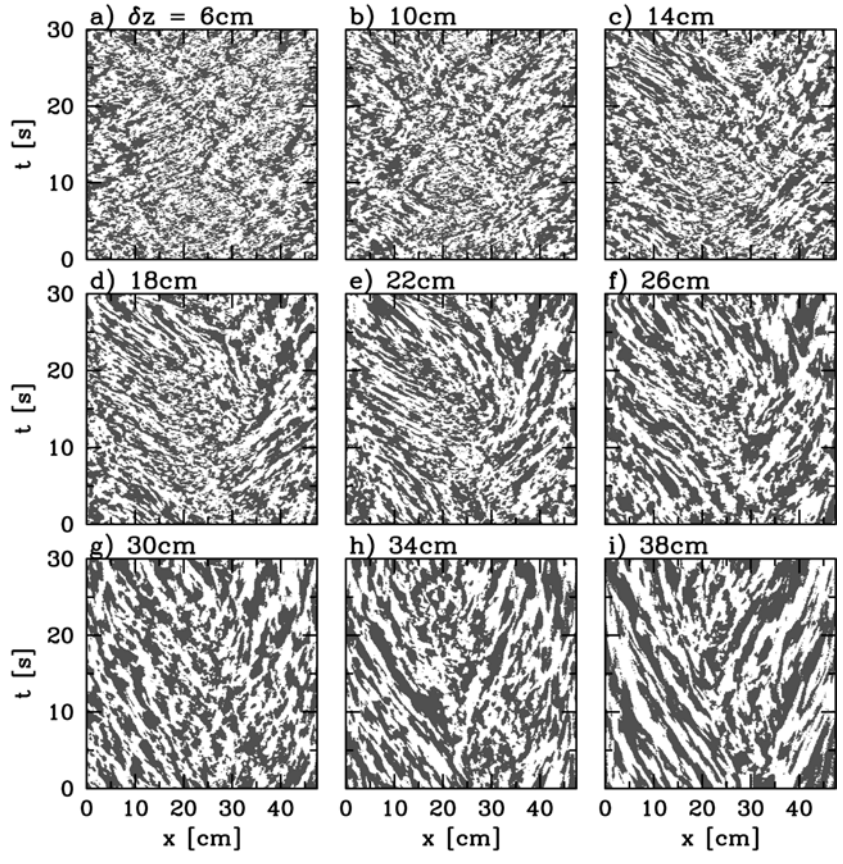

Fig. 4. Horizontal time series for an experiment with D=42 cm taken at locations 6–38 cm below grid, every 4 cm. A divergence from the centre of the tank to the sides is evident from the symmetric diagonal streaks of fluid. Intensities below the mean intensity value are marked as white, above the mean as gray

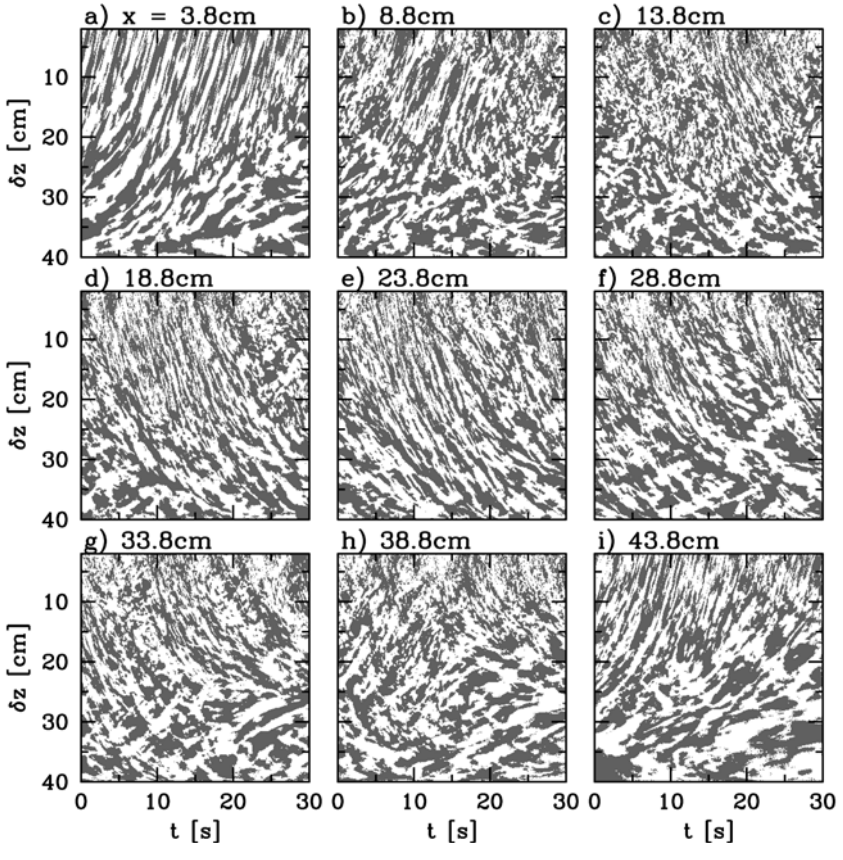

Fig. 5. Vertical time series for an experiment with D=42 cm taken every 5 cm across the front of the tank, starting 3.8 cm from the left edge of the tank. Streaks with positive slopes indicate upward motion of fluid, seen at the sides of the tank, and negative slopes indicate downward motion in the centre of the tank. The gray scale is defined in the same way as in Fig. 4

thin boundary layer extending approximately 2 cm from the side walls (with no mean flow along the front and back walls). Smaller scale eddies were embedded within this overall circulation and their associated time scales increased with distance away from the grid. This circulation was a robust feature in experiments with $D \gg W$. On a

slower time scale, transient upwelling near the centre of the tank was also sometimes observed. In experiments with large D, fluid upwelled from the bottom over significant patches far from the side walls. This upwelling phenomenon became more pronounced in experiments with progressively larger values of D, and the circulation pattern organized to form two counter-rotating cells as previously described.

In experiments where D was comparable to W, a large-scale circulation did not develop except within a small region at the side walls near the oscillating grid. Furthermore, the structure of the eddies embedded within the large-scale circulation changed as D varied. For $D \approx W$ the turbulence appeared to be approximately horizontally homogeneous.

These circulation patterns occurred whether the mixed region was bounded below by a rigid wall or by a deformable interface between the turbulent fluid and unmixed fluid of larger density. We ascribe the transition of the circulation pattern as D increased to a change between the turbulence behaving as though fully three-dimensional ($D \approx W$) and quasi-two-dimensional ($D \gg W$). In the latter case, the high horizontal aspect ratio of the tank restricted the development of isotropic eddies to length scales smaller than W. However, if D was large, turbulent motions with length scales larger than W acted as if they were two-dimensional. That is, there was no mean flow along the front and back tank walls. This circulation may have been enhanced by the relatively high grid frequency (7 Hz), which was the critical frequency at which secondary motions occurred in the experiments of McDougall (1979). The secondary motions were not, however, in the form of counter-rotating vortices.

Changes in turbulent properties when the depth of the mixed region rivals the horizontal dimensions of the tank have been previously observed. A change in the dynamics of a turbulent front in a homogeneous fluid was observed for $D > W$ in the cylindrical tank experiments of Dickinson and Long (1978). As well, in the two-layer experiments of Fernando and Long (1983), the deepening rate of the turbulent region showed a marked increase after the depth passed a breakpoint.

4
Scaling theory

The energy dissipation, ϵ, in a statistically steady forced turbulent flow scales according to

$$\varepsilon \frac{\tilde{u}^3}{\ell} \tag{8}$$

where u is the rms fluctuating velocity and ℓ is the integral length scale of the eddies (Tennekes and Lumley 1972).

In three-dimensional turbulence there is a transfer of energy from the integral length scale to the Kolmogorov microscale, η. The latter is the typical length scale at which kinetic energy is irreversibly dissipated through the action of molecular viscosity. The value of η is related to the energy dissipation rate by

$$\eta \propto (\nu^3/\varepsilon)^{1/4}. \tag{9}$$

Assuming the grid supplies energy evenly across the horizontal area of the tank at grid level, and assuming the tank dimensions do not affect the turbulence, the relevant vertical length scale characterizing the turbulence is δz, the distance below the energy source. In theory, δz is measured with respect to a virtual origin (Long 1978b; Thompson and Turner 1975). In practice we find that it is sufficient to take the virtual origin at the mean vertical position of the oscillating grid. Dimensional arguments then predict that $\ell \propto \delta z$ and $\eta \propto \delta z$. Combining these results with Eqs. (8) and (9), the velocity is found to scale with distance from grid as $u \propto \delta z^{-1}$. This scaling was also derived by Long (1978b), although using a different theoretical approach. This dependence has been documented experimentally (E and Hopfinger 1986) in tanks with square horizontal cross-sectional area.

The characteristic time scale, $\tau = \ell/u$, of horizontally homogeneous three-dimensional turbulence is thus expected to obey the scaling law

$$\tau_{3D} \propto \delta z^2. \tag{10}$$

The scaling for the experiments in which $D \gg W$ cannot be derived following the same dimensional arguments as in the three-dimensional case. Eddies that extend to sufficiently large depths increase in size until the extent is comparable to the tank width, W. Below this depth the eddies are constrained laterally and are thus free to move only in an approximately two-dimensional plane (the x, z plane). Since energy cascades to larger scale in two-dimensional turbulence (Fjørtoft 1953), the eddies continue to increase in size to fill the extent of the domain in which they are contained. Thus, a mean circulation develops.

However, the eddy motions at scales $\ell \ll W$ are not confined by the tank geometry and the turbulence at the small scales is still approximately isotropic in horizontal planes. This small-scale turbulence is advected and distorted by the mean circulation.

Therefore, as D is increased, there is a transition from three-dimensional unconstrained turbulence to quasi-two-dimensional turbulence at large scales with embedded three-dimensional small-scale turbulence. The dynamically important length scales are then D/W as well as δz, and the time scale dependence need not necessarily follow Eq. (10). Indeed, Hopfinger and Toly (1976) measured a distortion of the scaling given by Eq. (10) in the presence of a secondary flow.

5
Results

In this section we measure the variation of eddy time scales with depth from grid midplane and investigate how the structure of the turbulence changes for different values of D, which varies from 7.7 to 34.7 cm.

For each experiment, 27 vertical time series are taken across the tank, starting at 4 cm from the left wall, spaced 1 cm apart, to 30 cm from the left wall. The time series are collected sufficiently far from the side walls to avoid strong

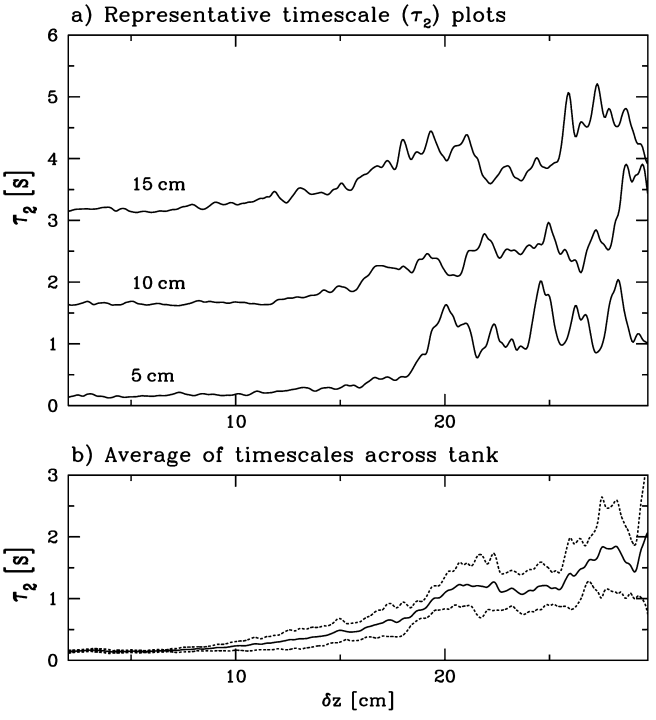

Fig. 6. **a** Three (vertical offset) plots of eddy time scales $\mathscr{T}_2$ as a function of distance from grid, δz, in an experiment with D=34.7 cm taken from time series at x=5, 10, and 15 cm. **b** Average and standard deviation (dotted line) of 15 time-scale profiles taken at successive horizontal positions across the tank

upward moving jets in the 2 cm wide boundary layer near the tank side walls. Time series far from the left wall of the tank are not used to measure time scales because of weak intensity signals resulting from light attenuation across the tank by the pearlescent dye.

In several large aspect ratio experiments, fluid upwelled near the centre of the tank. In these upwelling regions the turbulence was observed to evolve with much longer eddy time and length scales than those in the downwelling turbulence. For consistency, time-scale analyses are performed only where the centre motion is downward.

Time-scale analyses are performed individually on each of the (at most 27) time series. The resulting profiles of time scale versus depth are then averaged. For example, the time scales determined from an experiment with D=37.4 cm is shown in Fig. 6. Figure 6a shows three time-scale profiles calculated for the time series at 5, 10, and 15 cm from the left wall of the tank. The profiles are vertically offset for clarity. Along all three profiles the time scale generally increases with depth, though values fluctuate greatly for large δz. The fluctuations are reduced after averaging, as evident in Fig. 6b, which shows the average and standard deviation of 15 time-scale profiles across the width of the tank in the same experiment. The plot shows how the fluctuations in each time-scale profile are smoothed by the averaging process.

Log–log plots of the averaged time-scale profiles of $\mathscr{T}_1(\delta z)$ and $\mathscr{T}_2(\delta z)$ are shown in Fig. 7 for three experiments with D=14.6, 24.7, and 34.7 cm.

Particularly evident in the $\mathscr{T}_1$ results, but common to both time scales, are different scaling regimes of the turbulence. Crudely, we identify three regimes: a near-grid regime, a mid-depth regime, and a near-bottom regime. The first and second regimes occur approximately over the respective ranges δz=3–7 cm and δz=12–20 cm (when

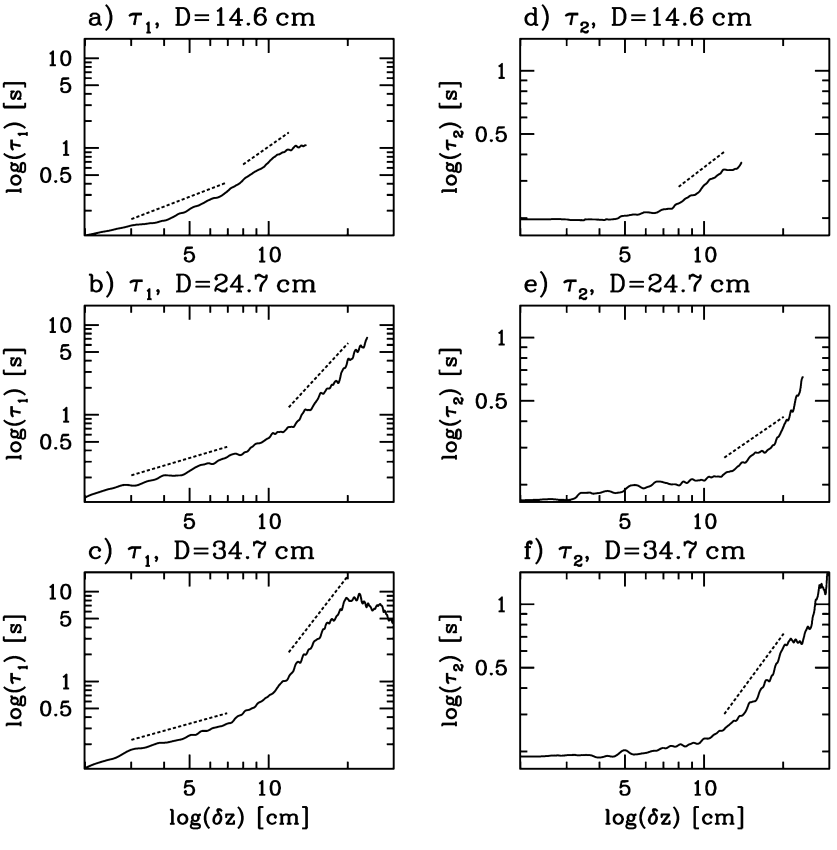

Fig. 7. Comparison of profiles for time scales $\mathscr{T}_2$ and $\mathscr{T}_1$. Log–log plots of eddy time scales $\mathscr{T}$ as a function of distance from grid δz for three depths of tank, D=14.6, 24.7, and 34.7 cm from grid midplane. The (vertically offset) best-fit lines to the plots are given for the ranges δz=8–12 cm when D=14.6 cm, and δz=12–20 cm when D=24.7, and 34.7 cm

$D \geq 20$ cm). These are distinguished by different power law dependencies of the form

$$\mathcal{T} = (\delta z)^p. \tag{11}$$

The power law exponent is smaller in the near-grid regime. Indeed, the time scale profiles characterized by $\mathcal{T}_1$ show a distinct elbow in all experiments, whereas with $\mathcal{T}_2$ the change is more gradual. In experiments with $D \gg W$, a third near-bottom regime is evident in which there is no power law dependence.

We measure δz from the midplane of the grid rather than from the virtual origin defined by Hopfinger and Toly (1976). Since the behaviour of the turbulence time scales near the grid is different from that away from the grid, the dependence of eddy time scale with δz cannot be meaningfully extrapolated to a virtual origin. In particular, the time scales characterized by $\mathcal{T}_2$ are approximately constant functions of δz near the grid and so cannot be extended to $\mathcal{T}_2 = 0$ to determine the virtual origin. Following Hopfinger and Toly (1976), the location of the virtual origin for our experimental configuration would be 1±0.5 cm below the midplane of the grid. Varying the location of the virtual origin by ±2 cm from the midplane of the grid resulted in a maximum of a 13% difference in the value of the exponent for the power law.

The $\mathcal{T}_1$ power law exponents, p, measured for $3 \leq \delta z \leq 7$ cm (=1–2 S) in a series of experiments with different depths, D, are denoted by diamonds in Fig. 8. The exponents are approximately constant over all values of D, with a value $p \approx 0.79 \pm 0.17$. This suggests that the structure of the turbulence in this range is affected exclusively by the jets from the mixer and not by the tank geometry, as evident in Fig. 4a. It has been extensively reported (Thompson and Turner 1975; Hopfinger and Toly 1976; Fernando and Long 1983; Atkinson, Damiani and Harleman 1987) that the individual wake and jet structure persists within two stroke lengths of the grid.

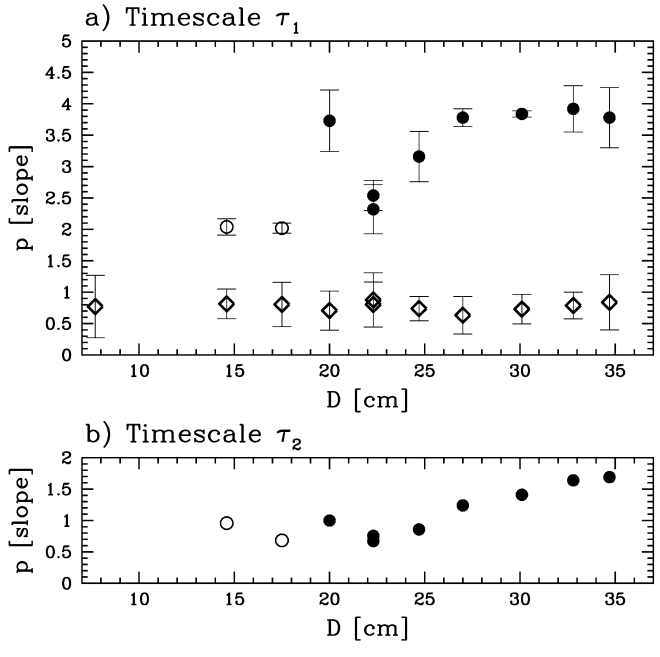

Fig. 8a, b. Power law dependence of time scale with distance from grid for experiments with varying depth of tank, D. **a** Timescale τ_1; **b** timescale τ_2. The different symbols represent different ranges of data used to calculate the slopes of the best-fit lines to the logarithmic plots of Fig. 7. *Solid circles*: δz=12–20 cm; *open circles*: δz=8–12 cm (the total depth of tank is less than 20 cm); *diamonds*: δz=3–7 cm. The error bars give the standard deviation of the best-fit lines. In **b** the error bars are within the size of the circles

At fast time scales, i.e. very close to the grid, $\mathcal{T}_1$ is sensitive to the resolution of the time series data. In order to test for the degree of sensitivity, we performed the analysis on the same data but at half the resolution. The results were qualitatively the same but with consistently lower values of power law in the near-grid regime and no change in the mid-depth values.

The power law exponents measured for $12 \leq \delta z \leq 20$ cm are denoted by the solid circles in Fig. 8 for both $\mathcal{T}_1$ and $\mathcal{T}_2$. In experiments with D<20 cm, the power law is instead computed over the range δz=8–12 cm. These results are denoted by the open circles in Fig. 8. The two data points at D=22.3 cm correspond to two different experiments at that depth of tank.

In the experiment with D=20 cm a large exponent is measured because the plot of $\mathcal{T}_1(\delta z)$ does not show a sharp distinction between near-grid and mid-grid regimes. The best-fit line in the common range of δz=12–20 cm used to establish the power law was taken at the curve in the plot similar to the elbows seen in Fig. 7.

When the ratio of D to W is approximately 1:1, the counter-rotating cells of the mean circulation are not observed, and the turbulence is expected to act as if it is fully three-dimensional. In experiments with progressively larger D, a large-scale circulation is more pronounced and the measured values of p are larger. Whether characterized by $\mathcal{T}_1$ or $\mathcal{T}_2$, generally we find that the power law exponent at mid-depth in the tank increases with increasing D.

These plots clearly demonstrate how the turbulent scaling at mid-depth is distorted by the presence of a bottom boundary, even though the boundary is many eddy length scales below the scaling region. The turbulence is affected by the large-scale circulation that develops and deviations from horizontally homogeneous turbulence theory become more pronounced in experiments with $D \gg W$.

The dynamics of the large-scale circulation is illustrated in Fig. 9 which shows the results of the cross-correlation analysis performed on an experiment with D=42 cm. While the time series in Figs. 4 and 5 qualitatively show the existence of the circulation, the cross-correlation effectively determines the slopes of the streaks in these images and so measures the velocities.

Typical velocities for the vertical motions are 2.0 cm/s for the overall downwelling motion and 1.5 cm/s for the return flow near the sides. The velocities are calculated at nine points using a Gaussian-weighted average of 506 velocities determined directly from the cross-correlation analyses. The accuracy in the final velocity measurement is determined from the standard deviation of the averaging process. The accuracy of the measured velocities ranges from 0.3 cm/s to 1.2 cm/s, depending on the intensity and duration of the streaks in the original time series. The

vertical velocities with accuracy close to 0.3 cm/s are those at the centre and sides of the tank. These are the regions where the vertical motion in the circulation is strongest and the cross-correlation signal is unambiguous.

Similarly, the magnitude of the horizontal velocities is typically 2.0 cm/s measured with an accuracy between 0.5 and 1.2 cm/s. The accuracy is poor at the centre and sides of the tank where the horizontal component of the velocity field is close to zero.

The cross-correlation analysis measures velocities of a strong mean circulation, such as that which occurs in the experiment with D=42 cm. In experiments with small D there is no significant mean circulation and such an analysis cannot be done.

6
Discussion and conclusion

We have shown that pearlescent dye is a useful tool for visualizing the qualitative features in a turbulent flow and for taking quantitative measurements. The dye can highlight individual eddy motions as seen, for example, by the increase in time scale from top to bottom of Fig. 3a. It can also highlight mean flows in the turbulence. For example, Figs. 4 and 5 clearly show two tank-scale counter-rotating vortices. Pearlescence also marks the boundary of a turbulent region, as in the deepening of the mixed region shown in Fig. 2.

We have developed a non-intrusive technique that uses pearlescent dye to measure the variation in time scale with distance from the energy source in oscillating grid turbulence over the entire flow field. This technique can be used to measure the local vertical and horizontal velocities of a mean flow in the turbulence.

We have found that the change in eddy time scales with distance from an oscillating grid exhibit different regimes. $\mathcal{T}_1$, which measures the strength of the jump discontinuity and the duration of the eddies, shows distinct near-grid and mid-depth power law scaling regimes. In the regime closest to the mixer, the time scales exhibit a power law dependence in which the exponent depends exclusively on the distance from the oscillating grid. In the intermediate-depth regime the slopes of the log–log plots increase with increasing depth of the tank. $\mathcal{T}_2$ is less sensitive to the temporal resolution, but a power law scaling is not as obvious. Nonetheless, using either of our definitions of eddy time scale we see the same increasing trend in the time-scale power law with an increase in D. Thus, we have found that the location of the bottom boundary affects the turbulence scaling behaviour over a distance much longer than the characteristic length scale of the eddies near the base of the mixing region.

We attribute the change in scaling behaviour to the observed development of a mean circulation which occurs if $D \gg W$. The circulation develops as a result of a transition from fully three-dimensional turbulence in the case where $D \leq W$ to quasi-two-dimensional turbulence in which there is an upscale cascade of energy for eddies with length scales larger than W. Embedded within this large-scale turbulence is the small-scale three-dimensional turbulence. The measured time-scales record the variability of eddies much smaller than the mean circulation. The observed increase in power law exponent with an increase in D is thus due to the transition from undistorted eddies to eddies distorted by the mean circulation.

Although the experiments described in this paper involve homogeneous fluid with a rigid bottom boundary, further experiments investigating a turbulent mixed layer overlying a stratified fluid have shown that similar dynamics occur when the rigid boundary is replaced with a stratified layer.

These experimental results may indirectly prove useful in interpreting turbulence measurements in the surface mixed region of the ocean. It is common practice to assume the classic "law-of-the-wall" for turbulence scaling in the oceanic boundary layer (Kantha and Clayson 2000). This assumes that scaling is a function only of distance from the surface. Our results show that scaling may also be affected by the depth of the thermocline underneath the oceanic boundary layer in the presence of a mean circulation, such as Langmuir circulations. These wind-induced circulations have the form of counter-rotating cells similar to the counter-rotating vortices observed in our experiments with large D. Though generated by a different mechanism, and despite the presence of a mean horizontal surface flow, our results suggest that the mean circulations distort the scalings in the turbulence.

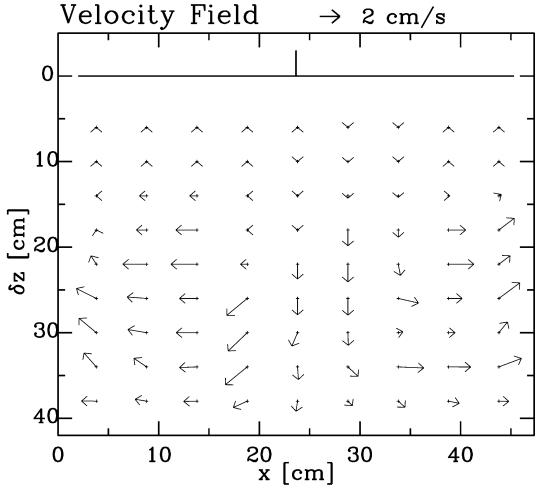

Fig. 9. The velocity field from cross-correlation analysis for the same experiment as in Figs. 4 and 5, in which counter-rotating cells are prominent. The depth of tank is D=42 cm. The velocity scale is illustrated by the *arrow* above the plot

References

Atkinson JF, Damiani L, Harleman DRF (1987) A comparison of velocity measurements using a laser anemometer and a hot-film probe, with application to grid-stirring entrainment experiments. Phys Fluids 30:3290–3292

Comte-Bellot G, Corrsin S (1971) Simple Eulerian time correlation of full- and narrow-band velocity signals in grid-generated "isotropic" turbulence. J Fluid Mech 48:273–337

Dalziel SB (1993) Rayleigh–Taylor instability: experiments with image analysis. Dyn Atmos Oceans 20:127–153

Dickinson SC, Long RR (1978) Laboratory study of the growth of a turbulent layer of fluid. Phys Fluids 21:1698–1701

Dickinson SC, Long RR (1983) Oscillating-grid turbulence including effects of rotation. J Fluid Mech 126:315–333

E X, Hopfinger EJ (1986) On mixing across an interface in stably stratified fluid. J Fluid Mech 166:227–244
Fernando HJS, Long RR (1983) The growth of a grid-generated turbulent mixed layer in a two-fluid system. J Fluid Mech 133:377–395
Fjørtoft R (1953) On the changes in the spectral distribution of kinetic energy for two-dimensional, nondivergent flow. Tellus 5:225–230
Hinze JO (1959) Turbulence. An introduction to its mechanism and theory. McGraw-Hill, New York
Hopfinger EJ, Toly JA (1976) Spatially decaying turbulence and its relation to mixing across density interfaces. J Fluid Mech 78:155–175
Kantha LH, Clayson CA (2000) Small scale processes in geophysical fluid flows. Academic Press, San Diego
Long RR (1978a) A theory of mixing in a stably stratified fluid. J Fluid Mech 84:113–124
Long RR (1978b) Theory of turbulence in a homogeneous fluid induced by an oscillating grid. Phys Fluids 21:1887–1888
McDougall TJ (1979) Measurements of turbulence in a zero-mean-shear mixed layer. J Fluid Mech 94:409–431
Tennekes H, Lumley JL (1972) A first course in turbulence. MIT Press, Cambridge, Mass.
Thompson SM, Turner JS (1975) Mixing across an interface due to turbulence generated by an oscillating grid. J Fluid Mech 67:349–368
Turner JS (1973) Buoyancy effects in fluids. Cambridge University Press, Cambridge
Voropayev SI, Fernando HJS (1996) Propagation of grid turbulence in homogeneous fluids. Phys Fluids 8:2435–2440